JMEPEG (2007) 16:500–507
DOI: 10.1007/s11665-007-9040-4

1059-9495/$19.00

Effect of Retained Austenite on GPM A30 High-Speed Steel

T.H. Yu and J.R. Yang

(Submitted January 21, 2006; in revised form May 29, 2006)

The amounts of retained austenite in the powder high-speed steel GPM A30 were calculated using a Rietveld computer model, and the relationship between the microstructure and hardness was studied. A test of the mechanical properties yielded the best heat treatment conditions and supported the production of high-quality A30 high-speed steel. The goal of this work was to estimate the amount of austenite retained following various heat treatments, and the mechanical properties of A30 P/M high-speed steel were further studied.

Keywords heat treating, high-speed steel, retained austenite, Rietveld method, x-ray diffraction

1. Introduction

The requirements of high-speed steel are diverse because they have a wide of range of applications. High-speed steels have good wear resistance, because they have a large volume fraction of undissolved carbides (Ref 1). High hardness at elevated temperatures is achieved and retained due to the precipitation of secondary hardening carbides (Ref 2). Under annealing conditions, high-speed steels have a ferrite matrix with a large amount of undissolved carbides. Under hardened conditions, they contain martensite, retained austenite, and undissolved carbides. Following tempering, which may be a multiple process, the structure contains tempered martensite, undissolved carbides, and a little retained austenite (Ref 3-8).

As-cast high-speed steels typically have a microstructure that comprises coarse primary carbides in a matrix of ferrite (Ref 9). Pronounced ingot segregation causes conventional tool steels commonly to contain a coarse, nonuniform microstructure with low transverse properties: and problematic size control and hardness uniformity under heat treatment (Ref 2). Powder metallurgy high-speed steels eliminate such segregation and have a fine homogeneous microstructure with uniformly distributed carbides and nonmetallic inclusions. Therefore, P/M high-speed steels are achieved with accompanying improvement in strength, toughness, out of-roundness distortion, grindability, and tool life (Ref 1).

The analytical method of this study is the RIETAN system. It is a software package that analyzes x-ray and neutron diffraction data measured with an angle-dispersive diffractometer using the Rietveld method (Ref 10, 11). Rietveld's open-handed sharing of all aspects of his work has supported great advances in our ability to extract detailed crystal structural information from powder diffraction data. Various researchers in the area of diffractometry thus realize that much more information can be applied to full-pattern analysis. The important point is that in a step-scanned pattern, for example, some information is attached to each intensity at each step in the pattern, even if it is the negative information that no Bragg-reflection intensity exists there, or the partial and initially scrambled information that the intensity at a step is the sum of contributions from the several Bragg reflections (Ref 12, 13). The x-ray diffraction data on elements and compounds shows the space groups of martensite, retained austenite, and carbides. Therefore, based on the lattice parameter of the phase and the results of x-ray diffraction, the amount of retained austenite is calculated.

The presence of multiple phases in a powder, revealed by its diffraction pattern, inevitably degrades the resolution of the data and, for the same total counting time, reduces the intensity of the pattern from each component. As a result, multiphase samples are an annoying and sometimes pathological problem in crystal structure refinement studies. However, Rietveld analysis of such mixtures has recently been determined to provide very accurate estimates of the relative and/or absolute abundance of the component phases.

This research focuses on the amount of retained austenite and its effect on the mechanical properties of A30 P/M high-speed steel.

2. Experimental Procedure

The P/M high-speed steel adopted herein was produced by Gloria Material Technology Corp. It is called P/M steel GPM A30. Its chemical composition was identified using a Spark-AES (JOBIN YVON JY48), carbon-sulfur determinator (LECO CS-244), and a nitrogen-oxygen determinator (LECO TC-136). Table 1 presents the details of the chemical composition.

Powdered A30 high-speed steel was hot isostatically pressed (sintering temperature = 1150 °C). The theoretical density of the ingot reached 97-100%. The compact powder samples were salt-bathed at various austenitizing temperatures for 180 s;

T.H. Yu and **J.R. Yang,** Department of Materials Science and Engineering, National Taiwan University, Taipei, Taiwan, ROC. Contact e-mail: d89542011@ntu.edu.tw.

Table 1 Chemical composition of GPM A30 high-speed steels (wt.%)

Fe	C	Si	Mn	P	S	Ni	Cr	Mo	V	W	Co	[N]	[O]
Bal.	1.28	0.44	0.28	0.021	0.022	0.22	4.18	5.00	3.20	6.13	8.73	794	174

[N] and [O]: ppm

quenched to room temperature in oil, and finally tempered at various temperatures for 120 min. Figure 1 presents the heat treatment process.

After heat-treatment, specimens were mechanically polished and analyzed using an X-ray diffractometer (PHILIPS PW1729). Since the reflected intensity was high, the step-scan mode was used to increase the relative intensity of all phases to yield an accurate calculation. Before analysis, the crystal structure, the space group, the lattice parameter, and the actual site occupied by the atom were to be prepared. This knowledge comes from International Tables for Crystallography Vol. A and the International Tables for X-ray Crystallography Vol. I presented in Table 2 (Ref 14, 15). The intensity data of x-ray diffraction were calculated using the Rietveld computer model. The amounts of retained austenite under various heat treatment conditions were thus calculated. Quantitative phase, or modal, analysis using the Rietveld method depends on the simple relationship designed by Hill and Howard (Ref 16-19), $W_p = \frac{S_p(ZMV)_p}{\sum_{i=1}^{n} S_i(ZMV)_i}$, where W is the relative weight fraction of the phase in a mixture of n phases, and S, Z, M, and V denote the Rietveld scale factor, the number of formula units per unit cell, the mass of the formula unit (in atomic mass units), and the unit cell volume (in $Å^3$), respectively. Figure 2 shows the analytical procedure (Ref 20).

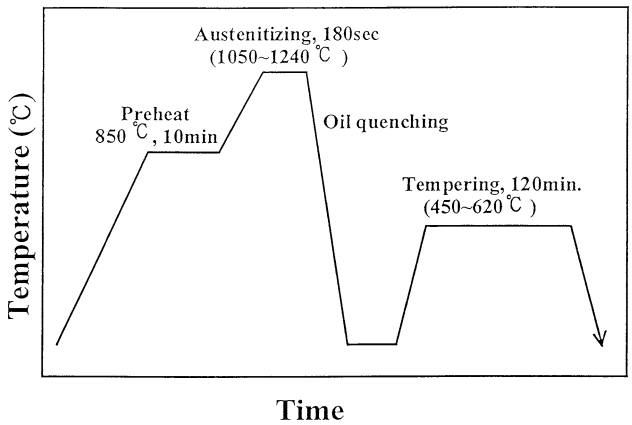

Fig. 1 The heat treatment process of GPM A30 high-speed steel

As well as being analyzed by x-ray diffraction, these specimens, obtained under various heat treatment conditions, were etched using 4% Nital solution to detect the optical morphology and measure the grain size of the pre-existing austenite, using the Snyder-Graff grain size number (Ref 9). Following the above, Rockwell hardness tests and transverse rupture strength tests were conducted on these ($7 \times 7 \times 65$ mm^3) specimens using a AKASHI MVK-EII Hardness Tester using a SHIMADZU Universal Testing Machine at a strain rate of 4 mm/min.

3. Results and Discussion

Table 3 presents the grain sizes measured in terms of Snyder-Graff grain size numbers. Figure 3 shows the actual grain sizes. The grains began to grow rapidly with the austenitizing temperature above 1160 °C, because all $M_{23}C_6$ ($Cr_{23}C_6$) carbides had already dissolved in the matrix and some M_6C ($Fe_3(W,Mo)_3C$ or $Fe_4(W,Mo)_2C$) carbides had also dissolved. Therefore, the obstacles hindered the growth of austenite, so the grains of the pre-existing austenite became larger. In this work, 1160 °C was selected as the austenitizing temperature for subsequent tempering heat treatment.

Figures 4 and 5 present the results of the x-ray diffraction experiment. Figure 4 refers to the quenching of specimens from 1050, 1160, and 1240 °C and Fig. 5 refers to quenching to 450, 500, and 620 °C from 1160 °C. MC carbides were identified as VC and M_6C carbides were identified as $Fe_3(W,Mo)_3C$ and $Fe_4(W,Mo)_2C$. Comparing the experimental peak lines with the theoretical peak lines enables the phases that corresponds to the peaks to be identified.

The Rietveld computation yields the relative amount of retained austenite which is given in Table 4. The amount of retained austenite increased with the austenitizing temperature. The results of the Rockwell hardness test yielded the relationship between the quenched hardness and the amounts of carbides and retained austenite. Figure 6 shows the amount of retained austenite and the quenched hardness versus austenitizing temperature. The amount of carbide that dissolves in the matrix increases with the austenitizing temperature, reducing the Ms temperature and stabilizing the retained austenite in the matrix. Therefore, the amount of retained austenite increased

Table 2 The lattice parameter and space group of different phases for Rieveld analysis (Ref 14, 15)

Phase	Martensite	Austenite	MC	M_6C	$M_{23}C_6$
Structure	b.c.c	f.c.c	b.c.c. (VC) h.c.p. (WC)	Diamond	f.c.c
Lattice parameter, Å	2.8665	3.5852	4.173 (VC) a = 2.907 (WC) c = 2.839 (WC)	11.0823	10.6214
Space group	I_{m3m}	F_{m3m}	F_{m3m} (VC)	F_{d3m}	F_{m3m}

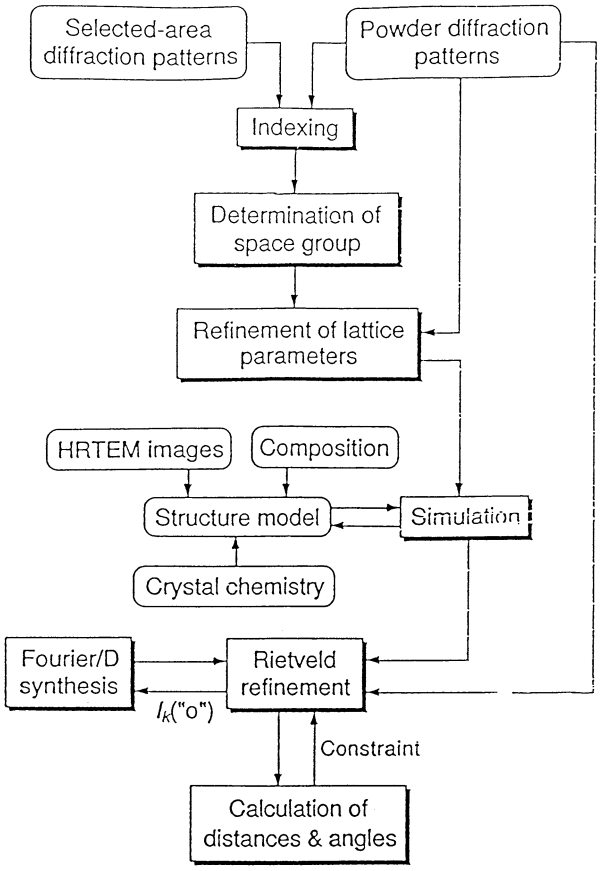

Fig. 2 The analytical procedure of the Rietveld method (Ref 20)

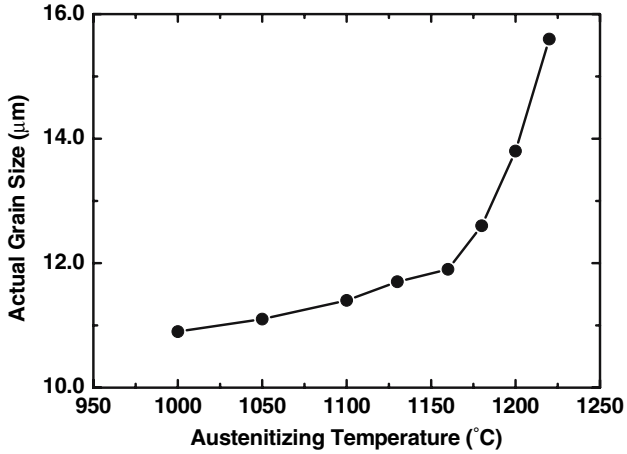

Fig. 3 The diagram of actual grain size vs. quenching temperature

with the austenitizing temperature. Powdered high-speed steels have high chromium, tungsten, vanadium, and molybdenum contents. Therefore, they exhibit characteristic secondary hardening. During tempering, carbon was dissolved during the austenitizing process, precipitating carbides and thereby strengthening the matrix. Table 5 presents the results of x-ray diffraction and the hardness test (for tempered specimens). Figure 7 shows the corresponding diagrams. The amount of retained austenite decreased as the tempering temperature increased. The curve of hardness versus tempering temperature revealed secondary hardening. The hardness reached a maximum at 500 °C, and then decreased gradually. The hardness of the specimens that were tempered at 500 °C exceeded the initial hardness of the untempered specimen (austenitized at 1160 °C). Tempering contributed to the decomposition of retained austenite and the precipitation of carbides from quenched martensite. The coherent strains established in the formation of these carbides were such that the resulting hardness more than overcame the softening caused by the depletion of carbon in the martensite. Therefore, the hardness increased overall. A further increase in tempering temperature transformed the retained austenite and supported the conversion of primary carbides to M_6C. Retained austenite decomposed to yield carbides and the Ms temperature was increased by the removal of alloying elements and carbon from the austenite, enabling the transformation of martensite upon cooling. Hardening that depended on the transformation of a large amount of retained austenite to martensite, was of limited value, because of the dimensional instability it caused. As the tempering temperature continued to increase, the carbides coarsened, so the hardness decreased.

Table 6 and Fig. 8 present the results of the transverse rupture strength test (fixed austenitizing temperature with various tempering temperatures). These tables and figures reveal a change in the transverse rupture strength (TRS) curves. Although the quenching temperatures varied, the transverse rupture strength was minimal at a tempering temperature of around 500 °C. This fact may be attributed to the precipitation of carbides and the formation of fresh martensite. When the tempering temperature was increased above 500 °C, carbides coarsened. The martensite (formed after quenching) was simultaneously tempered. Therefore, the toughness was improved.

As the quenching temperature increases, the TRS declined, because reducing the austenitizing temperature reduces the amount of retained austenite. The effect on toughness was slight. Besides, as the quenching temperature increased, the minimum TRS fell. Increasing the austenitizing temperature increases the amount of retained austenite, so the amount of fresh martensite increases after quenching.

Table 3 The Snyder-Graff size number of actual grain size and corresponding hardness of GPM A30 steel specimens after quenching from different austenitizing temperatures to room temperature

Quenching temp., °C	1000	1050	1100	1130	1160	1180	1200	1220
Size number	21.0	20.9	20.7	20.4	20.0	19.8	17.9	15.6
Hardness, HRc	69.0	68.2	67.4	66.2	65.9	65.6	64.9	64.7

P.S.: all values are mean value; the standard deviation of hardness is 0.5 HRc

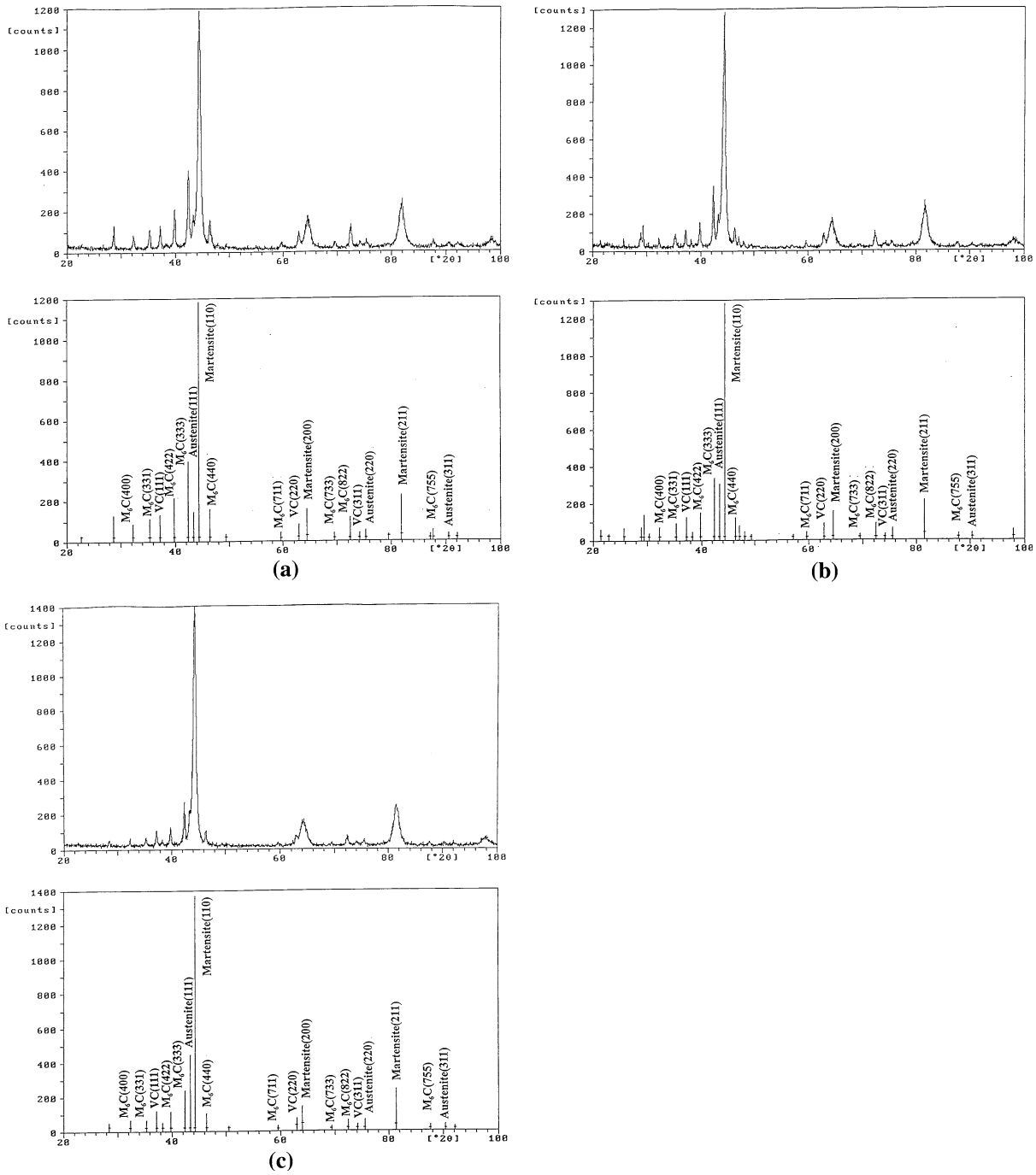

Fig. 4 The x-ray diffraction traces of A30 specimen after quenching from (a) 1050 °C; (b) 1160 °C; and (c) 1240 °C

Table 7 and Fig. 9 also present the results of the transverse rupture strength test (at a fixed tempering temperature with various austenitizing temperatures). When the tempering temperature was under 500 °C, increasing the austenitizing temperature reduced the TRS, for the following two reasons. First, the amount of retained austenite increased, so the amount of fresh martensite was higher after tempering. The brittleness of the fresh martensite makes TRS low. Second, the tempering temperature (<500 °C) was not sufficiently high to improve the toughness of the old martensite.

At a higher tempering temperature (>500 °C), when the austenitizing temperature exceeds 1130 °C, TRS is small. Since the effects of the tempered martensite and the fresh martensite were not balanced, the improvement of toughness by tempering could not compensate for the destruction due to the brittleness caused by decomposition. As the quenching temperature was slowly increased, more retained austenite decomposed into carbides and martensite. The resulting TRS became unfavorable.

When the quenching temperature was less than 1130 °C, a small amount of austenite was retained. A balance existed between toughness and brittleness. The increase in toughness by tempering was almost destroyed by the brittleness of fresh martensite. Therefore, the graph of TRS against temperature exhibited a steady state.

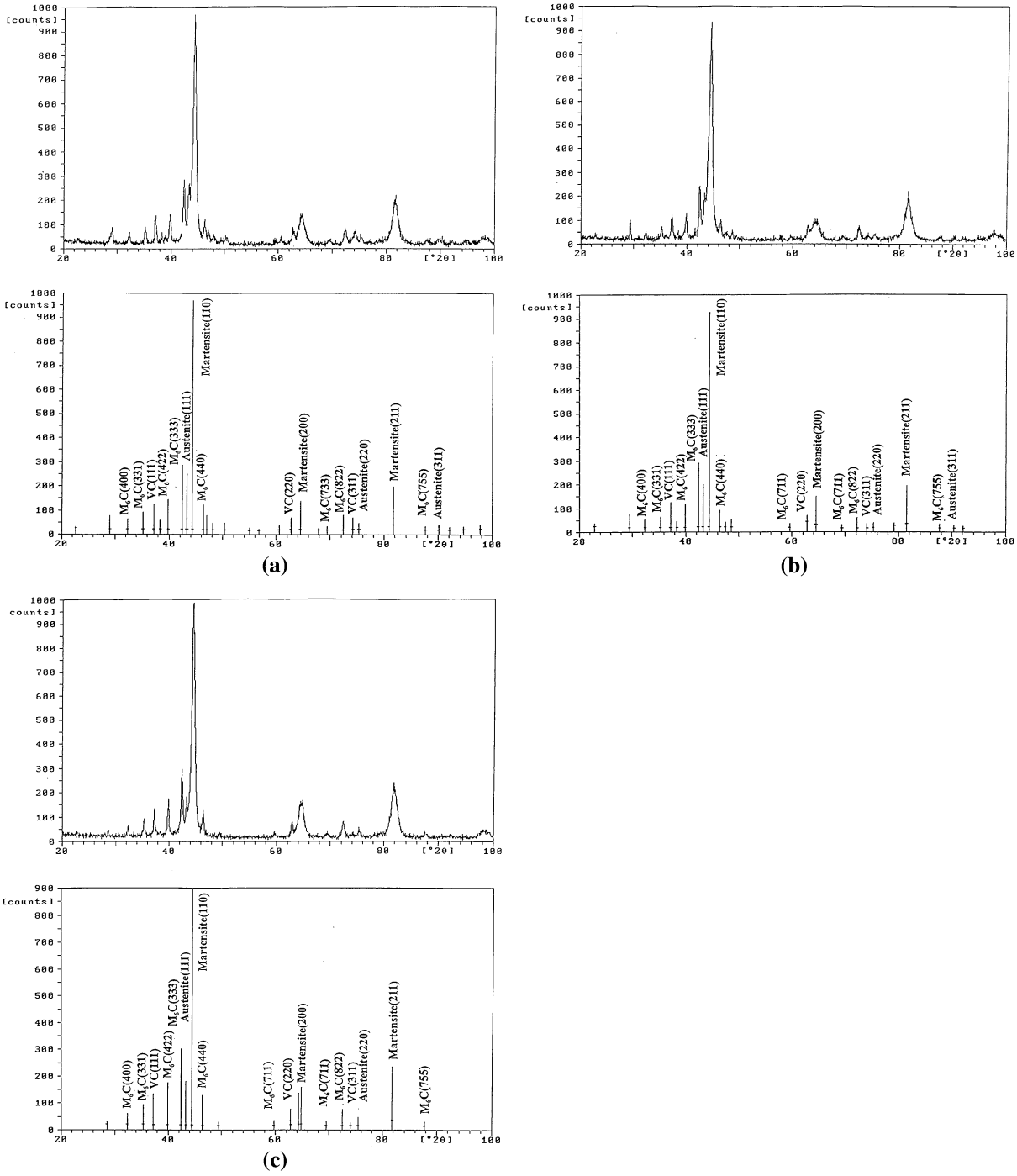

Fig. 5 The x-ray diffraction traces of A30 specimen tempered at (a) 450 °C; (b) 500 °C; and (c) 620 °C after quenching from 1160°C

Table 4 The amount of retained austenite (R.A.) and corresponding hardness of GPM A30 steel specimens after quenching from different austenitizing temperatures to room temperature

Quenching temp., °C	1050	1100	1130	1160	1180	1220	1240
R.A., %	7.3	10.2	12.6	15.6	17.7	20.0	22.2
Hardness, HRc	68.2	67.4	66.2	65.9	65.6	64.7	63.3

P.S.: all values are mean value; the standard deviation of R.A. is 0.5%, the standard deviation of hardness is 0.5 HRc

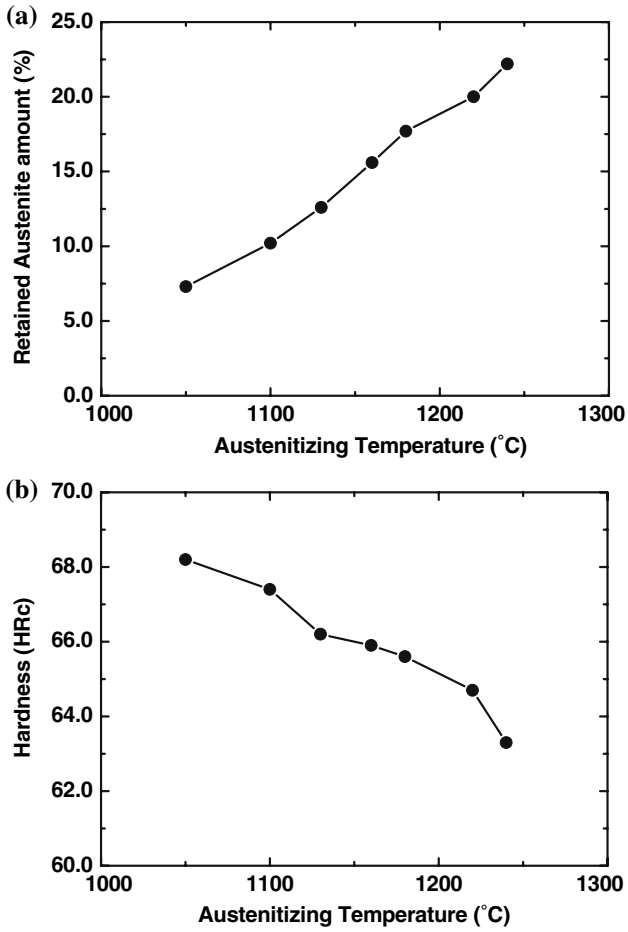

Fig. 6 Effect of austenitizing temperatures on (a) retained austenite amount (R.A. %) and (b) quenched hardness for A30 high-speed steel

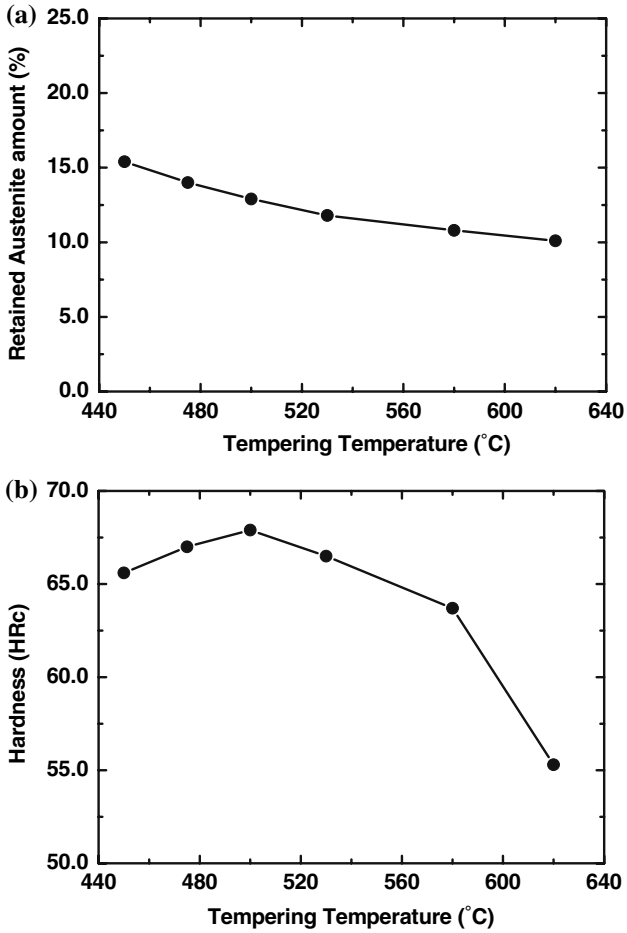

Fig. 7 Effect of tempering temperatures after quenching from 1160 °C on (a) retained austenite amount (R.A. %) and (b) tempered hardness for A30 high-speed steel

Table 5 The amount of retained austenite (R.A.) and corresponding hardness of GPM A30 steel specimens tempered at different tempering temperatures after quenching from 1160 °C

Tempering temp., °C	450	475	500	530	580	620
R.A., %	15.4	14.0	12.9	11.8	10.8	10.1
Hardness, HRc	65.6	67.0	67.9	66.5	63.7	55.3

P.S.: all values are mean value; the standard deviation of R.A. is 0.5%, the standard deviation of hardness is 0.5 HRc

Table 6 The transverse rupture strength (TRS) data of GPM A30 steel specimens tempered at different tempering temperatures after quenching from 1000 to 1220 °C

Tempering temp., °C	450	500	520	540	580	620	650
TRS, N/mm^2 at 1000 °C	1819	1528	1336	1330	1578	1741	1631
TRS, N/mm^2 at 1050 °C	1544	1318	1263	1492	1455	1537	1512
TRS, N/mm^2 at 1100 °C	1322	1245	1335	1364	1586	1572	1601
TRS, N/mm^2 at 1130 °C	1176	1056	1214	1401	1508	1392	1576
TRS, N/mm^2 at 1160 °C	1106	1015	1114	1197	1329	1412	1192
TRS, N/mm^2 at 1180 °C	1118	905	1062	1240	1236	1328	1222
TRS, N/mm^2 at 1200 °C	985	834	785	1066	1232	970	1090
TRS, N/mm^2 at 1220 °C	867	695	644	731	755	812	877

P.S.: all values are mean value

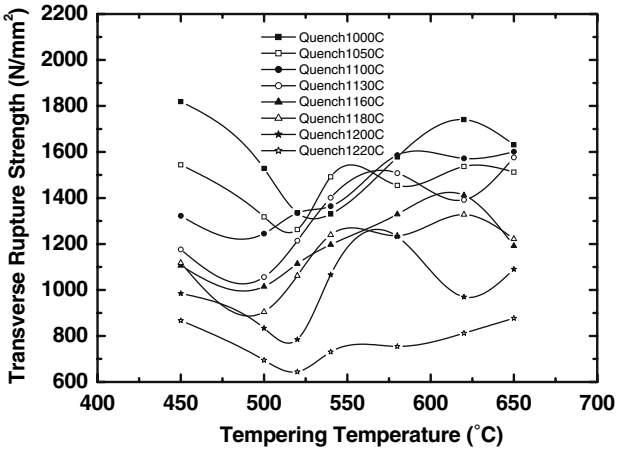

Fig. 8 Effect of fixed austenitizing temperature vs. different tempering temperatures on transverse rupture strength (TRS) for A30 high-speed steel

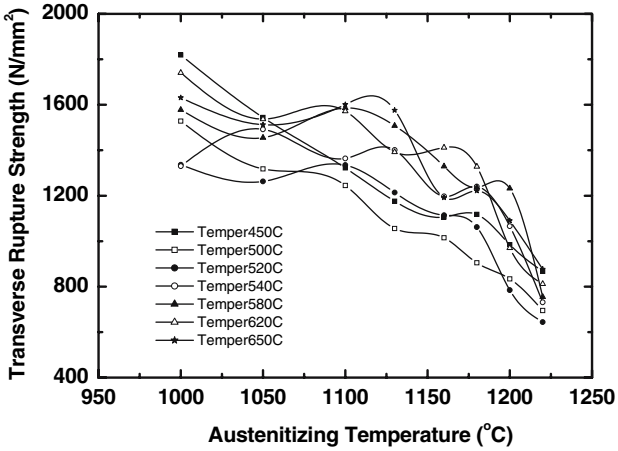

Fig. 9 Effect of fixed tempering temperature vs. different austenitizing temperatures on transverse rupture strength (TRS) for A30 high-speed steel

Table 7 The transverse rupture strength (TRS) data of GPM A30 steel specimens tempered at 450-650 °C after quenching from different austenitizing temperatures to room temperature

Quenching temp., °C	1000	1050	1100	1130	1160	1180	1200	1220
TRS, N/mm^2 at 450 °C	1819	1544	1322	1176	1106	1118	985	867
TRS, N/mm^2 at 500 °C	1528	1318	1245	1056	1015	905	834	695
TRS, N/mm^2 at 520 °C	1336	1263	1335	1214	1114	1062	785	644
TRS, N/mm^2 at 540 °C	1330	1492	1364	1401	1197	1240	1066	731
TRS, N/mm^2 at 580 °C	1578	1455	1586	1508	1329	1236	1232	755
TRS, N/mm^2 at 620 °C	1741	1537	1572	1392	1412	1328	970	812
TRS, N/mm^2 at 650 °C	1631	1512	1601	1576	1192	1222	1090	877

P.S.: all values are mean value

An earlier study established (Ref 2) that many practical conditions (such as external loading, increasing temperature, and deep cooling) transform retained austenite to martensite. Since such a phase transformation increases the volume, the dimensions and mechanical properties of tools would change. Therefore, many tempering processes have been used to reduce the level of retained austenite in the matrix. The product of tempering is well known to comprise ferrite, fresh martensite, carbides, and retained austenite. The fresh martensite formed by the transformation of retained austenite differed from that produced by earlier quenching treatment. The former martensite was fresh, brittle, and hard; the latter was tempered, and exhibited secondary hardening phenomenon with greater toughness.

4. Conclusions

1. The amount of retained austenite increased and the hardness of specimens decreased as the austenitizing temperature increased. The retained austenite simultaneously affected the dimensional stability of tool steel. Then, as the tempering temperature increased, the retained austenite decomposed to fresh martensite and carbides. Martensite, formed by an earlier quenching treatment, became tempered martensite. The hardness initially increased and then decreased as the tempering temperature was slowly increased.
2. At a given tempering temperature, TRS fell as the austenitizing temperature was increased.
3. At a given quenching temperature, TRS was minimal and hardness maximal at a tempering temperature of 500 °C.
4. At a given tempering temperature, TRS fell as the austenitizing temperature increased above 1130 °C.

References

1. T. Mukherjee, Physical Metallurgy of High-Speed Steels, *Proc. Conf. on Materials for Metal Cutting*, Apr. 14–16, 1970, iron and steel instp
2. G. Hoyle, *High Speed Steels*. 1st ed., Butterworth Press, Boston, 1988
3. R.J. Beltz, J.D. Dankoff, R.A. Heacox, and M.L. McClellan, Microstructure and Properties of High Speed Steels Produced from Solid State Microblended Powders, *Adv. Powder Metall., Novel Powder Processing*, 1992, **7**, p 369–381
4. B. Hribernik, K. Wurzwallner, H.P. Fauland, and G. Hackl, Investigation into the Microstructure and Mechanical Properties of an Advanced T15 Type PM High Speed Steel, *Proceedings of the 1990 Powder Metallurgy Conference and Exhibition Part 2 (of 3)*, May 20–23, 1990 (Pittsburgh, PA, USA), p 65–76
5. L.E.G. Cambronero, E. Gordo, J.M. Torralba, and J.M. Ruiz-Prieto, Comparative Study of High Speed Steels Obtained Through Explosive Compaction and Hot Isostatic Pressing, *Mater. Sci. Eng. A*, 1996, **A207**(1), p 36–45
6. Z. Guoli, H. Hengquan, and H. Fengming, Influence of Addition of High Speed Steel Powder on Properties and Structure of Sintered Steel, *Fenmo Yejin Jishu*, 1995, **13**(4), p 285–288 (in Chinese)

7. W. Graf, H.-J. Kraemer, J. Poetschke, and W. Weiglin, Production and Processing of High-Quality Powder Metallurgy Materials, *Powder Metall. Int.*, 1991, **23**(4), p 4
8. R. Waehling, P. Beiss, and W.J. Huppmann, Sintering Behaviour and Performance Data of High Speed Steel Components, *Powder Metall.*, 1986, **29**(1), p 53
9. G.A. Roberts and R. A. Cary, *High Speed Steels, Tool Steels*, 4th ed., American Society for Metals, Inc., 1980, p 627–761
10. H.M. Rietveld, Line Profiles of Neutron Powder Diffraction Peaks for Structure Refinement, *Acta Cryst.*, 1967, **22**, p 151–152
11. H.M. Rietveld, A Profile Refinement Method for Nuclear and Magnetic Structures, *J. Appl. Cryst.*, 1969, **2**, p 65–71
12. B.D. Cullity, *Elements of X-Ray Diffraction*, 2nd ed., Addison Wesley Publishing Company, Inc., 1978
13. R.A. Young, *The Rietveld Method*. 1st ed., Oxford University Press, New York, 1993
14. International Tables for Crystallography, Vol A, T. Hahn, Ed., D. Reidel Publishing Co., Boston, 1983
15. International Tables for X-ray Crystallography, Vol I, 2nd ed., N.F.M. Henry and K. Lonsdale, Ed., the Kynoch Press, Birmingham, England, 1969
16. R.J. Hill, Calculated X-ray Powder Diffraction Data for Phases Encountered in Lead/Acid Battery Plates, *J. Power Sources*, 1983, **9**(1), p 55
17. R.J. Hill and C.J. Howard, Quantitative Phase Analysis from Neutron Powder Diffraction Data Using the Rietveld Method, *J. Appl. Cryst.*, 1987, **20**, p 467
18. P.E. Werner, S. Salome, G. Malmros, and J.O. Thomas, Quantitative Analysis of Multicomponent Powders by Full-Profile Refinement of Guinier-Hägg X-ray Film Data, *J. Appl. Cryst.*, 1979, **12**, p 107
19. D.L. Bish and S.A. Howard, Quantitative Phase Analysis Using the Rietveld Method, *J. Appl. Cryst.*, 1988, **21**, p 86
20. F. Izumi, *Applications of Synchrotron Radiation to Materials Analysis*, Vol 405, H. Saisho and Y. Gohshi, Ed., Elsevier Science B. Press, New York, 1996